Two-Dimensional Beam Steering Using a Stacked Modulated Geodesic Luneburg Lens Array Antenna for 5G and Beyond

Pilar Castillo-Tapia, *Student Member, IEEE,* Oskar Zetterstrom, *Student Member, IEEE,* Astrid Algaba-Brazález, Lars Manholm, Martin Johansson, Nelson J. G. Fonseca, *Senior Member, IEEE,* and Oscar Quevedo-Teruel, *Senior Member, IEEE*

***Abstract*—Antennas for future communication systems are required to be highly directive and steerable to compensate for the high path loss in the millimeter-wave band. In this work, we propose a linear array of modulated geodesic Luneburg lens (the so-called *water drop* lens) antennas operating at 56-62 GHz. The lens array antenna features two-dimensional beam scanning with low structural complexity. The lenses are fully metallic and implemented in parallel plate waveguides, meaning that they are highly efficient. Each lens is fed with 13 rectangular waveguides surrounded by glide-symmetric holes to suppress leakage. The lenses provide 110 degree beam coverage in the H-plane with scan losses below 1 dB. In order to scan in the E-plane, we use a feeding network based on a 1:4 power divider and three phase shifters. In this configuration, the array can scan 60 degrees in the E-plane, albeit with higher scanning losses than in the H-plane. The lens array is manufactured and a good agreement between simulated and experimental results is obtained.**

***Index Terms*—Geodesic lens, lens antenna, linear array, Luneburg lens, multi-beam antennas.**

I. Introduction

New generations of communication systems intend to cover the requirements that higher data rates and lower latency that many emerging applications demand. In order to do that, a wider frequency spectrum allocation is needed [1]. Specifically for 5G, wide bands around 30 and 60 GHz were proposed to achieve high data rates [2]. The band at 60 GHz is mainly considered for short-range indoor scenarios due to its intrinsic high path losses. Therefore, antennas used in these applications need to compensate for these losses with high gain. To provide adequate angular coverage, the antennas must also be able to steer their directive beam.

A widely used antenna solution for directive beam scanning applications are planar phased arrays [3]. However, at millimeter-wave (mm-wave) frequencies, their feeding networks become complex and lossy [4]. Several methods have been proposed in the literature to simplify the feeding network of planar arrays. The most common one is to use beamforming networks, such as Butler matrices [5], [6], Blass matrices [7], [8] and Nolen matrices [9], [10], among others. However, for two-dimensional beam steering, these devices are often narrowband and complex. Alternatively, lenses can be added to a sparse array to simplify the feeding network while suppressing the grating lobes [11]. However, the scanning range is limited due to large scan losses. Another alternative is to use radomes that extend the scan angle [12], [13], which compromises the directivity in the broadside direction.

Fully-metallic planar lens antennas have also been proposed to provide high-gain and wide scanning at mm-wave frequencies [14]. In [15], a bifocal lens antenna implemented in a parallel plate waveguide (PPW) is proposed. The presented antenna can produce 11 fixed beams in a range of $\pm 30^{\circ}$. In [16], a double bifocal lens design is proposed, which increases the scanning range of this type of antenna ($\pm 50^{\circ}$). An even wider scanning range can be reached with a Luneburg lens antenna [17], [18]. This is due to the fact that the Luneburg lens is rotationally symmetric, which implies that the scan losses can be small. This lens antenna can be implemented with discretized layers of dielectrics [19] or through use of metasurfaces [20], [21]. The metasurfaces can be fully metallic to avoid the high material losses from dielectrics at high frequencies [22], [23]. However, due to the sub-wavelength size required for the unit cells, metasurface Luneburg lenses can be difficult to manufacture at higher frequencies.

Fully-metallic Luneburg lenses can also be implemented using geodesic profiles. These profiles are smooth, which alleviates the manufacturing constraints. Geodesic lenses are typically implemented using curved PPWs filled with a homogeneous material (such as air) that mimics the ray path of its refractive index counterpart [24]. This concept was introduced by Rinehart in [25] for the specific case of the Luneburg lens. Moreover, in [26], the analytical solution of the generalized geodesic Luneburg lens profile was presented. One drawback of this solution however is that the height of the lens is about one third of the lens diameter. As a result, conventional geodesic Luneburg lenses are bulky. In [27], it was proposed that this height can be reduced by folding the lens profile and in [28], an implementation of a folded

This work has been funded by the strategic innovation program Smarter Electronics System - a joint venture of Vinnova, Formas and the Swedish Energy Agency, under project High-Int (2019-02103) and by the European Space Agency in the frame of the Technology Transfer contract no. 4000130375/20/NL. The work of O. Quevedo-Teruel and P. Castillo-Tapia was also funded by the VR Project 2019-03933 under call "Research project grant within natural and engineering sciences".

P. Castillo-Tapia, O. Zetterstrom and O. Quevedo-Teruel are with the Division of Electromagnetic Engineering, KTH Royal Institute of Technology, SE-100 44 Stockholm, Sweden.

A. Algaba-Brazález, L. Manholm and M. Johansson are with Ericsson Research, Ericsson AB, Gothenburg 417 56, Sweden.

N. J. G. Fonseca is with the Antenna and Sub-Millimetre Waves Section, European Space Agency, 2200 AG, Noordwijk, The Netherlands.

Manuscript received XXXX; revised XXXX.

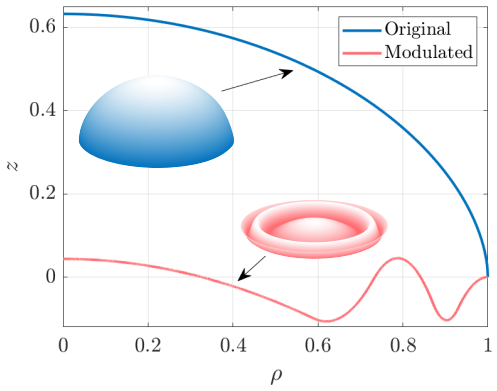

Fig. 1. Conventional and modulated geodesic Luneburg lens profiles and 3D surfaces (dimensions are normalized to the lens radius).

geodesic lens antenna was presented in which the sharp folding points in the lens profile are approximated with arcs to reduce reflections at the cost of moderate phase aberrations. This implementation reduced the height by 40% when compared to the conventional geodesic Luneburg lens. Recently, an efficient method to design modulated geodesic lens antennas has been presented in [18]. This modulated lens is referred to as the *water drop* lens and has contributed to a regain of interest in geodesic lenses for a number of applications at mm-wave frequencies [29]. The profile is defined by continuously differentiable functions, meaning that the folding is accounted for in the design, thus reducing the phase aberrations compared to [28]. Moreover, in [30], the integration of a polarizer at the flare of a geodesic lens antenna was proposed for dual-polarization applications. While geodesic lens antennas provide relatively simple manufacturing and high efficiency, these PPW lens antennas can only scan in one plane, which is not sufficient in some applications.

Here, we present a vertically stacked array of four *water drop* lens antennas. Stacking geodesic lenses was previously proposed in [30], but no demonstration of the scanning capabilities has been reported until now. The lens element is a scaled version of the lens in [18]. The lens antenna array is able to scan in two planes through beam switching in the horizontal plane and beam scanning in the vertical plane. Each lens antenna can produce 13 independent beams in an angular range of $\pm 55°$ in the horizontal plane with negligible scan losses thanks to the rotational symmetry of the lenses. Moreover, the linear array of four lenses allows to scan $\pm 30°$ in the vertical plane. This antenna benefits of the high efficiency and simplicity in the feeding network associated with geodesic lens antennas while enabling two-dimensional beam steering.

This article is organized as follows. Section II explains the design process of a single water drop lens antenna. In Section III, the lens array antenna is presented, including the design of a feeding network that includes a power divider and phase shifters. Section IV describes the experimental results of the lens array antenna and Section V summarizes the main conclusions.

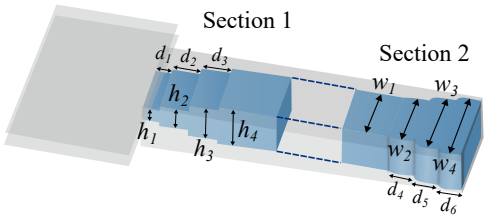

Fig. 2. Stepped transition from PPW to standard WR19 waveguide in two sections (height and width).

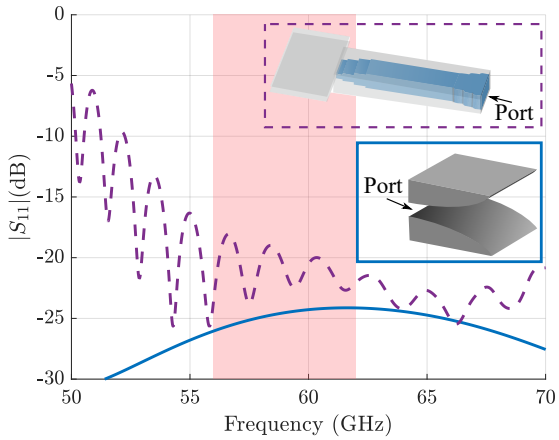

Fig. 3. Simulated reflection coefficient of the flare (blue line) and of the waveguide-to-PPW transition (purple dashed line). The parameters of the waveguide feed are reported in Table I.

II. Water Drop Lens Antenna Design

The designed array element is composed of a water drop lens integrated with 13 waveguide feeds and a flare. The waveguide feeds match the impedance of a standard WR19 waveguide to the PPW that forms the lens. On the other side, the flare impedance matches the lens to free space and its height is constrained by the separation between array elements.

A. Lens design

Luneburg proposed a rotationally-symmetric graded-index lens that has one focal point at the contour of the lens and one at infinity [17]. This lens transforms a cylindrical wave at any point on its surface into a plane wave at the opposite side. The refractive index of this lens is $n(\rho) = \sqrt{2-\rho^2}$, where ρ is the normalized radial position. The lens has a refractive index of $\sqrt{2}$ at the centre that gradually changes to 1 at the contour, meaning that it is matched to the free space impedance.

This graded refractive index can be mimicked by a geodesic profile with constant refractive index. The geodesic profile for a Luneburg lens is [25], [26]

$$dz = d\rho \sqrt{\left(\frac{1}{2} + \frac{1}{2\sqrt{1-\rho^2}}\right)^2 - 1} \tag{1}$$

where z the normalized height. This profile is plotted in Fig. 1 in blue together with its 3D surface. The height of this geodesic curve is around 0.63 times the radius of the

TABLE I
DIMENSIONS OF THE STEPPED TRANSITION.

Parameter	Dimension (mm)	Parameter	Dimension (mm)	Parameter	Dimension (mm)
h_1	0.8	w_2	3.483	d_3	1.654
h_2	1.315	w_3	4.218	d_4	1.368
h_3	2.048	w_4	4.8	d_5	1.357
h_4	2.39	d_1	0.914	d_6	1.305
w_1	3.2	d_2	1.592		

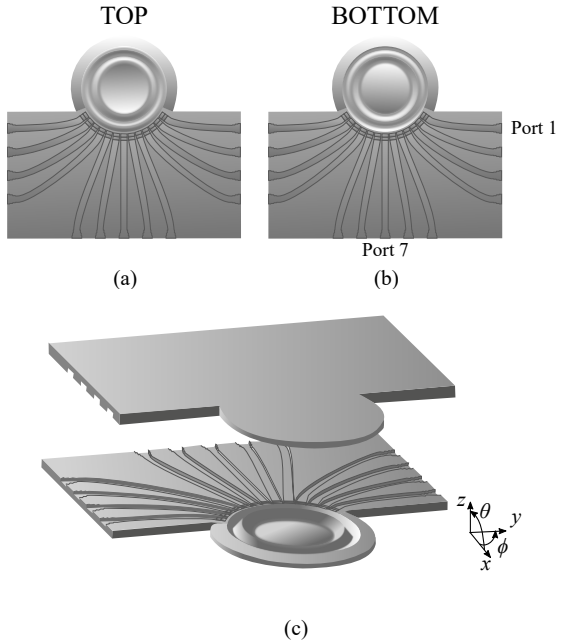

Fig. 4. Designed water drop lens antenna: (a) upper plate, (b) bottom plate and (c) exploded view of the antenna.

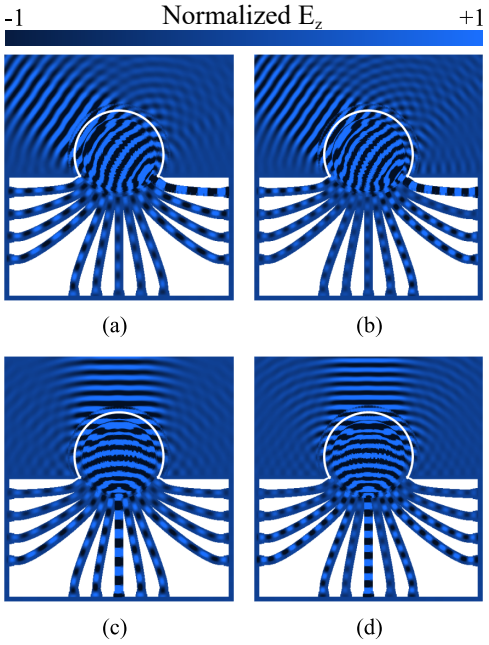

Fig. 5. Electric field distribution when exciting: (a) port 1 at 56 GHz, (b) port 1 at 62 GHz, (c) port 7 at 56 GHz, and (d) port 7 at 62 GHz.

lens, which can be too bulky for some applications. The lens response can be mimicked more compactly with a modulated surface profile (water drop) as the one illustrated in pink in Fig. 1 [18]. This modulated profile has a height ~ 0.24 times more compact than the original geodesic profile.

In this work, we use the modulated profile from [18], with a radius of $4\,\lambda_0$ at 57 GHz (21 mm). A PPW is formed with the pink profile in Fig. 1 corresponding to the profile of the mean surface between the two metallic surfaces, which are separated here by a distance of 0.8 mm. This separation is less than $0.2\,\lambda_0$ at the highest frequency (62 GHz), ensuring that only the fundamental PPW mode can propagate over the frequency band of operation.

B. Ports and flare design

Rectangular waveguides are used to feed the lens. Each rectangular waveguide is stepped, as illustrated in Fig. 2, in order to match the impedance of the waveguide to the PPW. The stepped transition is designed in two sections to match the dimensions of a standard WR19 waveguide for test purposes. In the section closest to the PPW (section 1), the height is modified to match the impedances of the waveguide and the PPW, while in the section close to the port (section 2), the width of the waveguide that is modified. The width of the waveguide is not modified close to the lens due to the

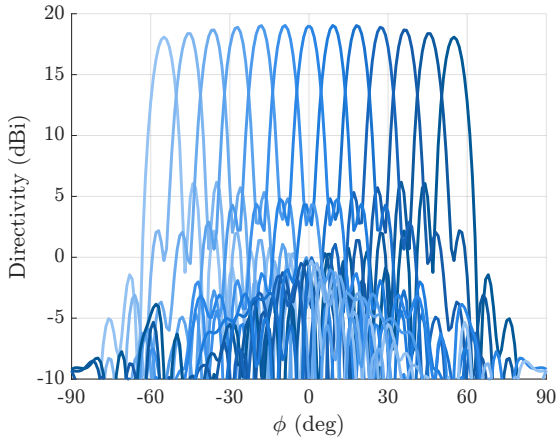

Fig. 6. Simulated H-plane radiation patterns at 60 GHz for a single water drop lens antenna.

limited space. The two matching sections are connected by a uniform waveguide whose length does not have a relevant impact on its operation. The steps that increase the width are rounded in the corners with a radius of 0.3 mm to account for manufacturing using milling. The optimized dimensions of the transition are reported in Table I and the reflection coefficient is presented with the purple dashed line in Fig. 3. The stepped

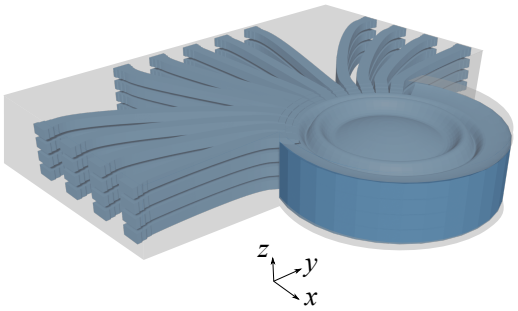

Fig. 7. Water drop lens array antenna with four stacked elements.

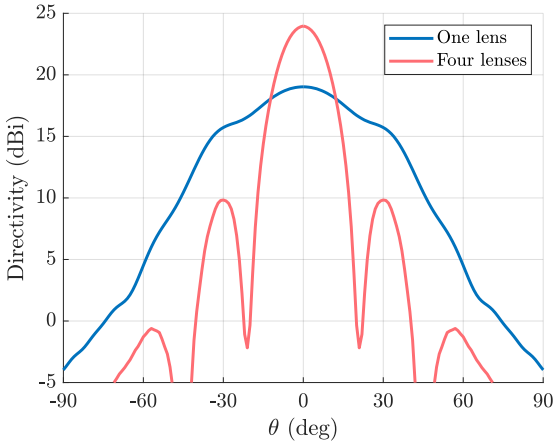

Fig. 8. E-plane radiation pattern of one and four stacked lenses at 60 GHz.

waveguide has a reflection coefficient below -15 dB in the band of operation (56-62 GHz).

To mitigate the reflections at the output of the lens, a flare is used to match the impedance of the PPW to the free space impedance. The lens is intended to be used in a vertical array, and therefore the height of the flare must be sufficiently small to avoid grating lobes when scanning. In our case, the targeted vertical scanning range is $\pm 30°$ and so the height at the output of the flare is chosen to be 3.5 mm (0.7λ at 60 GHz). The flare has a spline curved shape and a length of 5.24 mm. This flare is illustrated in the inset of Fig. 3. The reflection coefficient of the flare is presented with blue solid line in Fig. 3 and is below -20 dB in the band of interest.

C. Integrated lens antenna

Fig. 4 illustrates the integration of the 13 waveguide feeds and the flare with the lens. Fig. 4a and 4b show the upper and bottom plates of the lens, while Fig. 4c illustrates how the plates are combined to form the lens antenna. The waveguide feeds are extended to flat surfaces for testing purposes. These extensions, added between the two sections of the transition design, are smooth to minimize reflections. The feeds are spaced 9.2°, which means that the antenna can scan in a range of $\pm 55°$ in azimuth.

The z component of the electric field, E_z, is illustrated in Fig. 5 for port 1 and 7 (numbering indicated in Fig. 4) at 56 and 62 GHz. A plane wave is produced at 55° from port 1 and 0° from port 7 in the horizontal plane. Fig. 6 shows the simulated radiation patterns at 60 GHz. The maximum directivity and side lobe level (SLL) are 19.04 dB and -12 dB, respectively. A scanning range of $\pm 55°$ is achieved with a maximum scan loss of 0.96 dB. The worst-case crossover level is -5.5 dB.

III. Lens Array Antenna

The water drop lens antenna presented in Section II can only scan in one plane. In this section, we propose stacking these single elements in order to produce an array antenna that can scan in both azimuth (thanks to the lens) and elevation (thanks to the array), corresponding to the angles ϕ and θ, respectively, with the notations in Fig. 4. In this section, we propose an array composed of four lenses. This array is fed with a power divider and phase shifters that control the pointing angle in elevation. We note that, as a consequence of manufacturing tolerances, air gaps can occur between the stacked layers. In order to make our design robust to manufacturing errors, we introduce an electromagnetic band gap (EBG) structure to the design to mitigate against leakage, as previously implemented in [31].

A. Lens array design

The designed lens array antenna with four identical stacked lenses is illustrated in Fig. 7. It is interesting to note that the stack of lenses has a height of 16.7 mm, which is smaller than a single conventional geodesic Luneburg lens with the same diameter. Fig. 8 presents the radiation patterns in the E-plane at 60 GHz for a single lens element and the stacked array. The amplitudes and phases of the array are uniformly distributed and the patterns correspond to the ports that produce a beam at 0° in azimuth. The array has 6 dB higher directivity and the half-power beamwidth decreases from 53.1° to 18.3°, compared to the single lens element. The SLL in the E-plane of the array is -14 dB, as expected from the uniform amplitude distribution.

B. Array feeding network

A feeding network, composed by a 1:4 power divider and phase shifters, is designed to demonstrate the scanning capabilities of the lens array antenna. The main design parameters of the power divider and phase shifters are illustrated in Fig. 9.

The simulated S-parameters of the power divider are shown in Fig. 10. The reflection coefficient at the input port (port 1 in Fig. 9a) is below -20 dB in the band of interest, under the condition that ports 2 to 5 are matched. To reduce SLL in the E-plane of the lens array antenna, we design the power divider to produce a tapered amplitude distribution at its output ports. In our design, the transmission coefficients for ports 3 and 4 are equal to -5 dB at the design frequency whereas for ports 2 and 5, their value is set to -7 dB. The path length between the input port and all output ports is equalized resulting in a phase difference between output ports lower than 0.15°, which is in the order of the numerical accuracy of the model. This means that the power divider can be used to produce beams at 0° in elevation, without the external phase shifters.

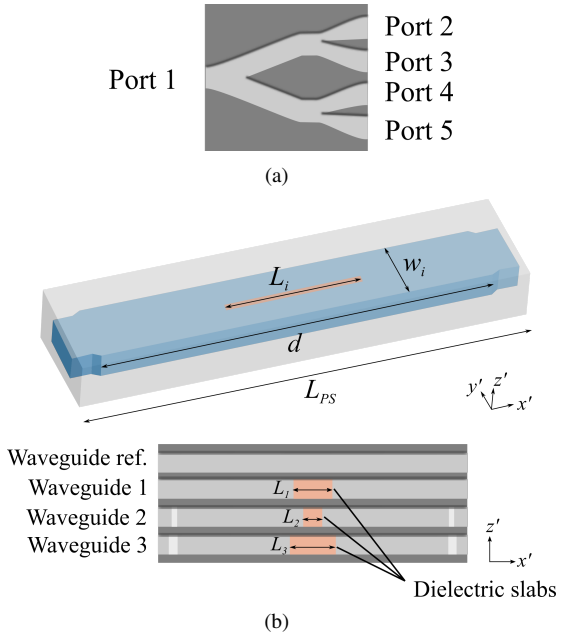

Fig. 9. Feeding network composed by (a) a 1:4 power divider and (b) phase shifters. The phase shifts are achieved by having a different waveguide width and varying the length of a dielectric slab placed in the middle.

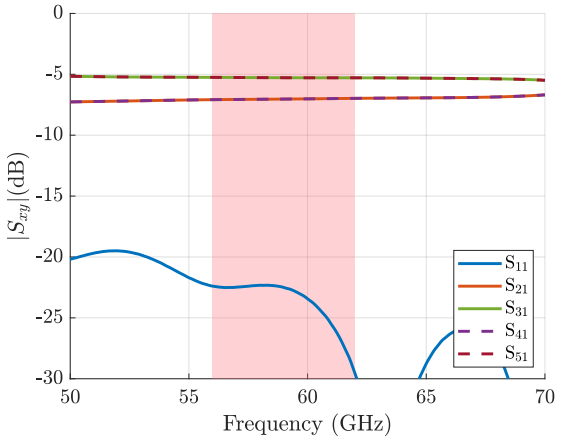

Fig. 10. Reflection and transmission coefficient of the designed power divider.

To scan the beam in elevation, phase shifting waveguides are connected to each of the output ports of the power divider. For demonstration purposes, fixed phase shifters are designed. In Fig. 10, the top waveguide is invariant in the x' direction and is used as a reference. In the remaining waveguides, different phase shifts are achieved by changing their width and the length of thin dielectric slabs placed at $y' = 0$, as proposed in [32]. The parameters are $L_{PS} = 40$ mm, $d = 35$ mm, $w_1 = 4.8$ mm, $w_2 = 5.6$ mm and $w_3 = 6$ mm. The dielectric slabs are made of Rogers RT5880 with thickness 0.508 mm. To scan 15º, slabs of length $L_1 = 3.5$ mm, $L_2 = 2.5$ mm and $L_3 = 5.6$ mm are used. To scan 30º, slabs of length $L_1 = 12$ mm, $L_2 = 16$ mm and $L_3 = 26.5$ mm are used. Fig. 11 shows the phase difference between each phase shifting waveguide and the reference waveguide. A progressive phase of 65º and 126º is required for scanning to 15º and 30º, respectively.

Fig. 12 shows the simulated E-plane radiation patterns for

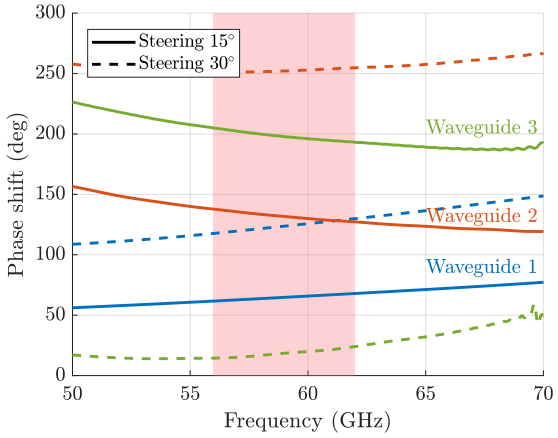

Fig. 11. Phase shifts for scanning 15° (with $L_1 = 3.5$ mm, $L_2 = 2.5$ mm and $L_3 = 5.6$ mm) and 30° (with $L_1 = 12$ mm, $L_2 = 16$ mm and $L_3 = 26.5$ mm). The parameters are $L_{PS} = 40$ mm, $d = 35$ mm, $w_1 = 4.8$ mm, $w_2 = 5.6$ mm and $w_3 = 6$ mm.

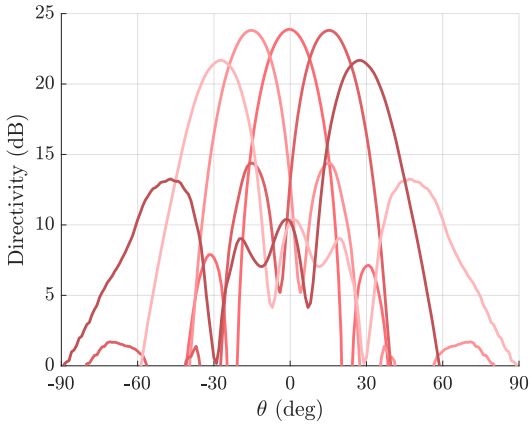

Fig. 12. E-plane radiation patterns of port 7 at 60 GHz.

the lens array when connecting the feeding network to the waveguide feeds that produce a beam at 0º in azimuth. The beam at 0º in elevation is obtained without the phase shifters. The other directions are obtained connecting the lens array antenna with the power divider and its corresponding set of phase shifters. The maximum directivity is 23.9 dB and the scan losses at 30° are 2.2 dB, following the cosine-like scan losses in linear arrays.

C. EBG implementation

An EBG structure can be placed surrounding each waveguide feed to avoid undesired leakage due to manufacturing tolerances. For example, metallic pins have already been proposed in a technology known as *gap waveguides* [33], [34]. Avoiding this leakage is especially critical in mm-wave bands [35]. Here, instead of metallic pins we have chosen to use glide-symmetric holes as the EBG structure [36], [37], [38]. These holes have demonstrated to be a robust solution for waveguides at high frequencies [39]. The proposed unit cell is shown in Fig. 13a. The holey structure used in this design has a period $p = 2.5$ mm, a radius $r = 1$ mm and a height $h = 1.5$ mm.

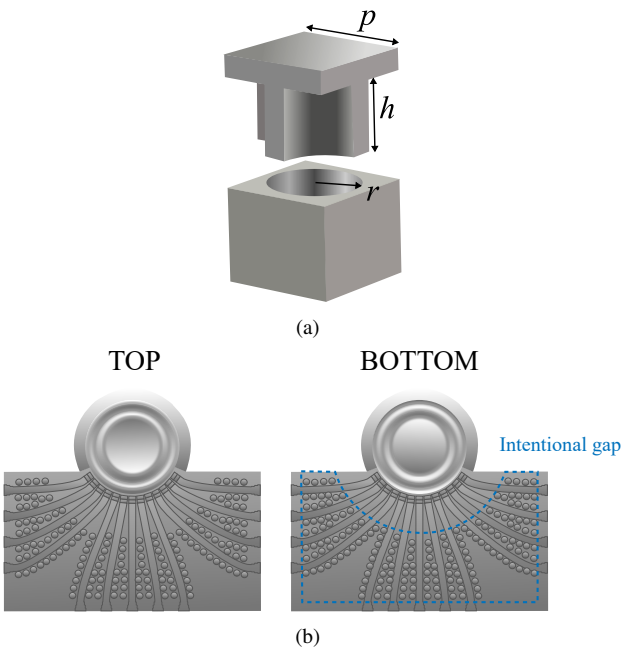

Fig. 13. (a) Unit cell of the glide-symmetric holes. (b) Top and bottom plate of the lens with glide-symmetric holes and an intentional gap in the region protected by the holes.

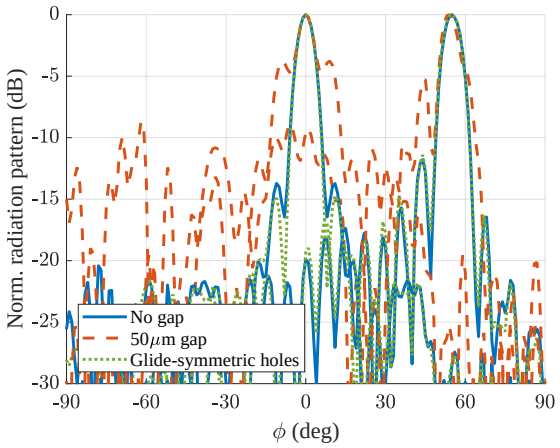

Fig. 14. Simulated radiation patterns at 60 GHz of ports 1 and 7. Comparison of no gap, and uniform gap of 50 μm with and without glide-symmetric EBG.

To illustrate the effect on the antenna performance due to undesired leakage, we have simulated a single water drop lens with an intentional uniform gap of 50 μm between the two plates. This uniform gap is obviously a worst case from a mechanical point of view as gaps are expected to be smaller and more localized; however the sensitivity of the structure to very small gaps shows the importance of the EBG structure. Fig. 14 reports the simulated radiation patterns of port 1 and 7 at 60 GHz for three different cases: 1) ideal case (no gap), 2) uniform gap of 50 μm between plates and 3) intentional gap of 50 μm including a glide-symmetric holey EBG structure. Fig. 13b shows the placement of the holes on the top and bottom plates that form a single lens antenna. To minimize the crossover between beams in azimuth, the waveguides must be placed as close as possible to each other on the contour of the

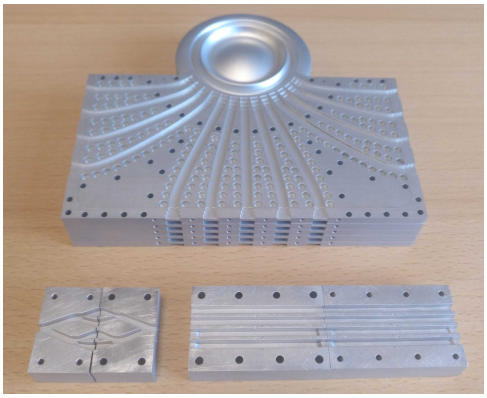

Fig. 15. Manufactured prototype including lenses (top), power divider (bottom left) and phase shifters (bottom right).

lens. Therefore, at the vicinity of the lens, there is not enough space for the EBG structure. For these simulations, we assume that there is no gap in this region. This is a good assumption in a real implementation, since a good contact between the two plates near the lens can be ensured if an intentional gap in the area protected by the glide-symmetric holes is imposed [31].

The results in Fig. 14 show that the uniform gap of 50 μm has a clear impact on the radiation patterns. For example, in port 1, this gap produces an increase of the SLL to -5.3 dB, and for port 7 to -3.8 dB, which is unacceptable for the targeted applications. Instead, the radiation patterns with the EBG structure have a similar performance than the no-gap case, validating the proposed mechanical design.

IV. Experimental Results

A prototype is manufactured using high-precision milling to verify the concept of the water drop lens array antenna. The prototype is shown in Fig. 15 with four array elements. More elements could be added at the top or bottom of the stack to increase the aperture size in elevation if required thanks to the generic layer design. The lens array antenna is composed of five identical plates milled on both top and bottom faces with an intentional gap of 20 μm in the areas protected by the glide-symmetric holes (see Fig. 13b). The manufactured feeding network is also shown in Fig. 15. Both power divider and phase shifters are produced in two parts, and the parts are joined in the E-plane. Therefore, the leakage resulting from manufacturing tolerances will be minimized thanks to symmetries.

The simulated and measured reflection coefficient of seven ports of a single lens array element are presented in Fig. 16. The results of the remaining six ports are omitted due to symmetry. Fig. 16a shows that the simulated reflection coefficients are below -17 dB in the band 56-62 GHz. Fig. 16b shows that the measured reflection coefficients for one lens antenna are below -10 dB in the band of interest. These discrepancies are attributed to the complexity of the antenna and manufacturing tolerances at these high frequencies. Similar results were achieved for the other array elements. The reflection coefficients of the lens antenna are measured connecting each

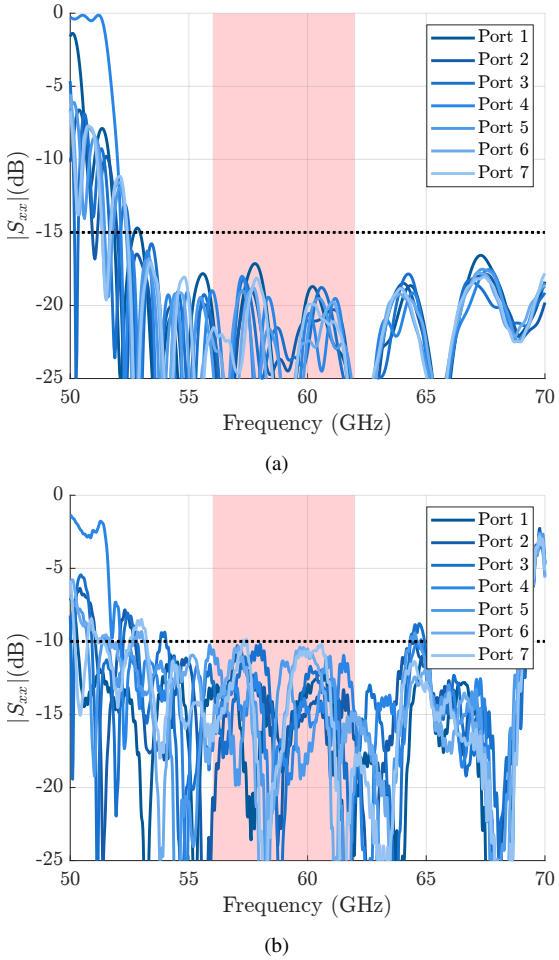

Fig. 16. (a) Simulated and (b) measured reflection coefficients. The measurements have been time-gated to remove the effect of the commercial coax-to-waveguide transition.

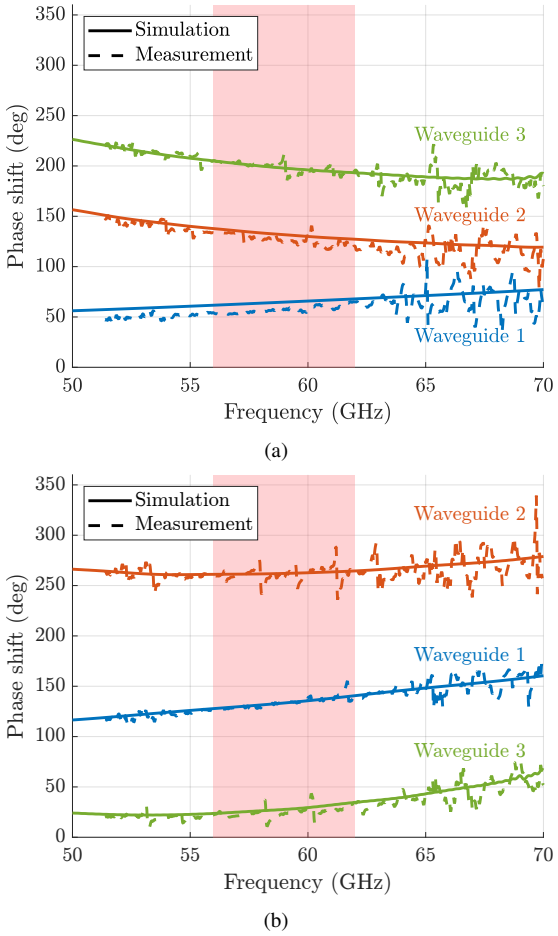

Fig. 17. Simulated (solid lines) and measured (dashed lines) phase shifts for steering a) 15° and b) 30°.

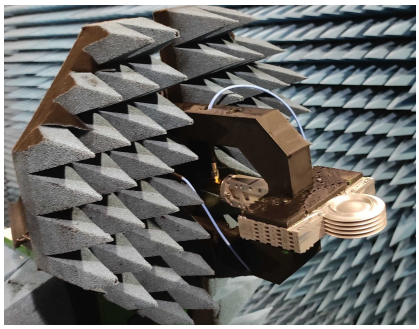

Fig. 18. Measurement setup in the anechoic chamber.

port to a commercial coax-to-waveguide transition. The results are time-gated to remove the effect of the transition.

Fig. 17 shows the simulated and measured phase shifts required for scanning to 15º and 30º in elevation. The phase shifts are relative to the reference waveguide. The simulations and measurements agree, apart from small peaks in the measurements. These peaks are due to the difficulty in placing the dielectric slabs straight.

The lens array antenna prototype is tested in the anechoic chamber of KTH. The measurement setup is depicted in Fig. 18. The radiation pattern is measured in a half sphere. Fig. 19 shows the normalized H-plane radiation patterns when the array is fed with uniform phase distribution at 56 and 62 GHz. This means that no phase shifter is used. The SLL is below -10 dB in all ports at both frequencies.

Fig. 20 shows the simulated (solid lines) and measured (dashed lines) 3 dB contour plots. The measurements are done for seven ports and the phases of the lens elements are configured to point to 0º, 15º and 30º in the E-plane. The remaining contour plots are symmetric and were not acquired as a complete characterization is time consuming. The beams have an average beamwidth of 6º in the H-plane and 20º in the E-plane. The simulations and measurements agree at both 56 and 62 GHz, apart from some discrepancies in the pointing angle. The measured beams intended to be pointing to 30º in elevation instead point at 25º. The discrepancies are attributed to manufacturing tolerances in the prototype that can cause undesired phase shifts between the elements. The simulated (solid lines) and measured (dashed lines) realized gains are shown in Fig. 21 for the considered beam pointing directions in the band of 56-62 GHz. When the array points at 0º in elevation (Fig. 21a), the simulated peak gain varies from 22.7 to 24.1 dBi. When the array points at 15º (Fig. 21b), the simulated peak gain varies from 22.2 to 23.7 dBi. When the array points at 30º (Fig. 21c), the simulated peak gain

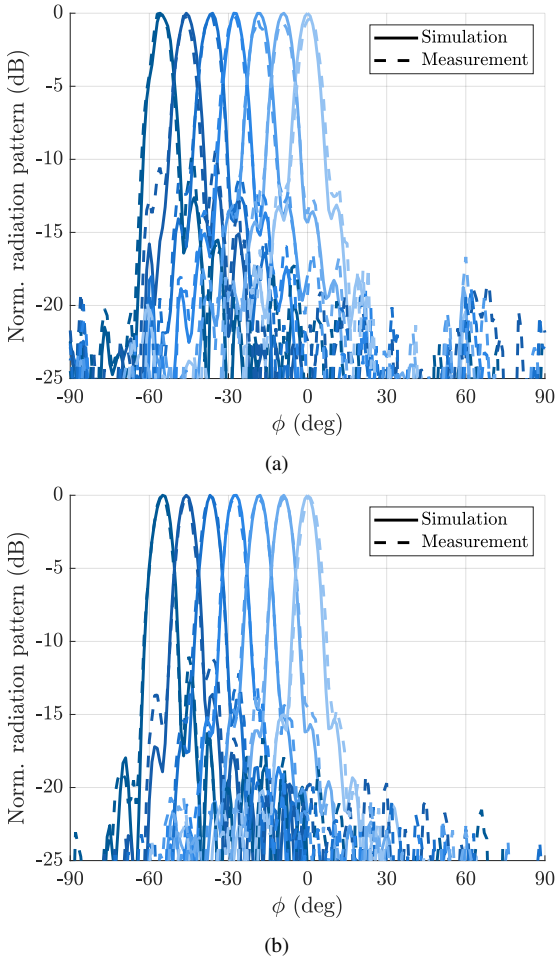

Fig. 19. Simulated (solid lines) and measured (dashed lines) normalized radiation patternsin the H-plane with uniform array excitation at (a) 56 GHz and (b) 62 GHz.

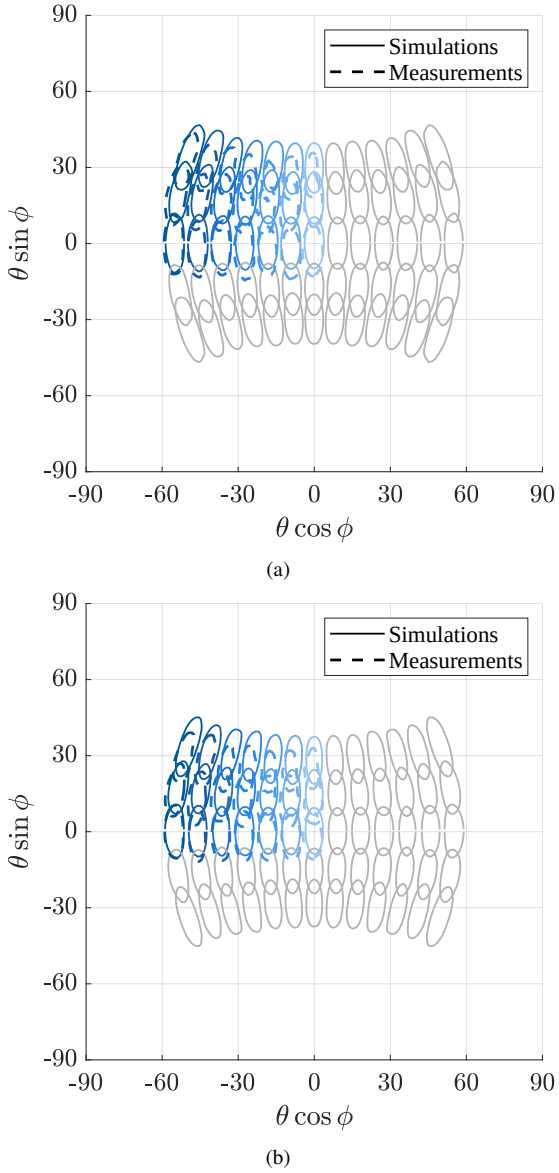

Fig. 20. Simulated (solid lines) and measured (dashed lines) normalized radiation patterns. Contour plots show -3 dB level at (a) 56 GHz and (b) 62 GHz.

varies from 20.2 to 21.3 dBi. This means that the maximum scan losses are within 2.5-2.8 dB. The measured gain is 1-2.5 dB lower than in the corresponding simulation for all beam pointing directions. These discrepancies in gain are attributed to the surface roughness in the prototype, which was not considered in the initial simulations and proved to be higher than anticipated. A simulation of port 1 with 3 μm of roughness provides a better agreement with the measurements. These results demonstrate the ability of the lens array to produce a high gain beam which can be steered in two planes.

V. Conclusion

In this work, we demonstrated the possibility of steering a beam both in azimuth and elevation using an array of stacked *water drop* lens antennas. The array consists of four lens antennas with an interelement separation of 0.7λ at 60 GHz. Each lens has 13 waveguide feeds and a flare is used to provide impedance matching to free space. Glide-symmetric holes have been added around the waveguide feeds to avoid leakage due to manufacturing tolerances. The lens antennas produce beams covering a $\pm 55^{\circ}$ range with 9.2° separation in the H-plane and have negligible scan losses. A feeding network is used to steer the beam $\pm 30^{\circ}$ in the E-plane. The feeding network is composed of a 1:4 power divider and phase shifters. To prove the concept, the phase shifters are designed to steer 15° and 30° in elevation.

The proposed array antenna is manufactured using milling and tested. The antenna operates in the band 56-62 GHz with reflection coefficients lower than -10 dB and measured peak gain of 22.5 dB. The lens antennas can steer $\pm 55^{\circ}$ in the H-plane, with 13 discrete beams. The array antenna can scan $\pm 30^{\circ}$ in elevation. The maximum scan losses are 2.5-2.8dB across the band. The simulations and measurements agree well.

The proposed solution features low complexity since the beamforming in one plane is done by the lens. A switching matrix may be added for applications requiring single beam. Moreover, the scan losses in one plane are also reduced thanks to the rotational symmetry of the lens.

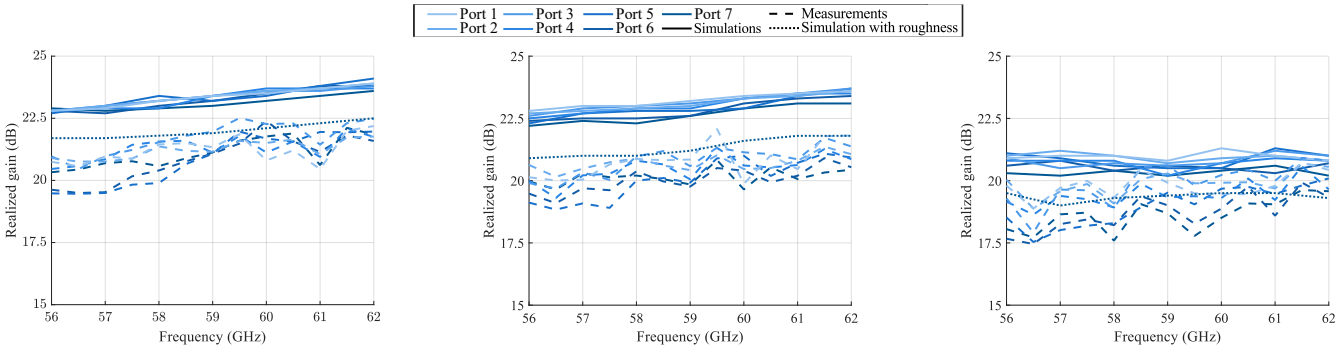

Fig. 21. Simulated (solid lines) and measured (dashed lines) realized gain scanning (a) 0º, (b) 15º and (c) 30º. The dotted line is a simulation of port 1 with 3 μm of roughness.

REFERENCES

[1] S. Parkvall, E. Dahlman, A. Furuskar, and M. Frenne, "NR: The new 5G radio access technology," *IEEE Commun. Stand. Mag.*, vol. 1, no. 4, pp. 24–30, 2017.

[2] A. Osseiran, S. Parkvall, P. Persson, A. Zaidi, S. Magnusson, and K. Balachandran. (April 2020) 5G wireless access: an overview. [Online]. Available: https://www.ericsson.com/en/reports-and-papers/white-papers/5g-wireless-access-an-overview. Accessed: 4 April 2022.

[3] J. Zhang, X. Ge, Q. Li, M. Guizani, and Y. Zhang, "5G millimeter-wave antenna array: Design and challenges," *IEEE Wirel. Commun.*, vol. 24, no. 2, pp. 106–112, 2017.

[4] R. Garg and A. S. Natarajan, "A 28-GHz low-power phased-array receiver front-end with 360° RTPS phase shift range," *IEEE Trans. Microw. Theory Tech.*, vol. 65, no. 11, pp. 4703–4714, 2017.

[5] J. Butler, "Beam-forming matrix simplifies design of electronically scanned antennas," *Electron. Des.*, vol. 9, pp. 170–173, 1961.

[6] T. Djerafi and K. Wu, "A low-cost wideband 77-GHz planar Butler matrix in SIW technology," *IEEE Trans. Antennas Propag.*, vol. 60, no. 10, pp. 4949–4954, 2012.

[7] J. Blass, "Multidirectional antenna - a new approach to stacked beams," in *Proc. IRE Int. Conv. Rec.*, vol. 8, 1960, pp. 48–50.

[8] P. Chen, W. Hong, Z. Kuai, and J. Xu, "A double layer substrate integrated waveguide Blass matrix for beamforming applications," *IEEE Microw. Wirel. Compon. Lett.*, vol. 19, no. 6, pp. 374–376, 2009.

[9] J. Nolen, *Synthesis of Multiple Beam Networks for Arbitrary Illuminations.* South Bend, IN, USA: Bendix Corporation, 1965.

[10] T. Djerafi, N. J. G. Fonseca, and K. Wu, "Broadband substrate integrated waveguide 4×4 nolen matrix based on coupler delay compensation," *IEEE Trans. Microw. Theory Tech.*, vol. 59, no. 7, pp. 1740–1745, July 2011.

[11] H. Zhang, S. Bosma, A. Neto, and N. Llombart, "A dual-polarized 27 dBi scanning lens phased array antenna for 5G point-to-point communications," *IEEE Trans. Antennas Propag.*, vol. 69, no. 9, pp. 5640–5652, 2021.

[12] A. Benini, E. Martini, S. Monni, M. C. Viganò, F. Silvestri, E. Gandini, G. Gerini, G. Toso, and S. Maci, "Phase-gradient meta-dome for increasing grating-lobe-free scan range in phased arrays," *IEEE Trans. Antennas Propag.*, vol. 66, no. 8, pp. 3973–3982, 2018.

[13] E. Gandini, F. Silvestri, A. Benini, G. Gerini, E. Martini, S. Maci, M. C. Viganò, G. Toso, and S. Monni, "A dielectric dome antenna with reduced profile and wide scanning capability," *IEEE Trans. Antennas Propag.*, vol. 69, no. 2, pp. 747–759, 2021.

[14] O. Quevedo-Teruel, M. Ebrahimpouri, and F. Ghasemifard, "Lens antennas for 5G communications systems," *IEEE Commun. Mag.*, vol. 56, no. 7, pp. 36–41, 2018.

[15] F. Doucet, N. J. G. Fonseca, E. Girard, X. Morvan, L. Le Coq, H. Legay, and R. Sauleau, "Shaped continuous parallel plate delay lens with enhanced scanning performance," *IEEE Trans. Antennas Propag.*, vol. 67, no. 11, pp. 6695–6704, 2019.

[16] T. Ströber, S. Tubau, E. Girard, H. Legay, G. Goussetis, and M. Ettorre, "Shaped parallel-plate lens for mechanical wide-angle beam steering," *IEEE Trans. Antennas Propag.*, vol. 69, no. 12, pp. 8158–8169, 2021.

[17] R. K. Luneburg, "Mathematical theory of optics," *Providence, Brown University Press*, 1944.

[18] N. J. G. Fonseca, Q. Liao, and O. Quevedo-Teruel, "Equivalent planar lens ray-tracing model to design modulated geodesic lenses using non-Euclidean transformation optics," *IEEE Trans. Antennas Propag.*, vol. 68, no. 5, pp. 3410–3422, 2020.

[19] A. N. Korotkov, S. N. Shabunin, and V. A. Chechetkin, "The cylindrical Luneburg lens discretization influence on its radiation parameters," in *2017 International Multi-Conference on Engineering, Computer and Information Sciences (SIBIRCON)*, 2017, pp. 394–398.

[20] C. Pfeiffer and A. Grbic, "A printed, broadband Luneburg lens antenna," *IEEE Trans. Antennas Propag.*, vol. 58, no. 9, pp. 3055–3059, Sept. 2010.

[21] J.-M. Poyanco, O. Zetterstrom, P. Castillo-Tapia, N. J. G. Fonseca, F. Pizarro, and O. Quevedo-Teruel, "Two-dimensional glide-symmetric dielectric structures for planar graded-index lens antennas," *IEEE Antennas Wirel. Propag. Lett.*, vol. 20, no. 11, pp. 2171–2175, 2021.

[22] O. Quevedo-Teruel, J. Miao, M. Mattsson, A. Algaba-Brazalez, M. Johansson, and L. Manholm, "Glide-symmetric fully metallic Luneburg lens for 5G communications at Ka-band," *IEEE Antennas Wirel. Propag. Lett.*, vol. 17, no. 9, pp. 1588–1592, 2018.

[23] H. Lu, Z. Liu, Y. Liu, H. Ni, and X. Lv, "Compact air-filled Luneburg lens antennas based on almost-parallel plate waveguide loaded with equal-sized metallic posts," *IEEE Trans. Antennas Propag.*, vol. 67, no. 11, pp. 6829–6838, 2019.

[24] R. C. Mitchell-Thomas, O. Quevedo-Teruel, T. M. McManus, S. A. R. Horsley, and Y. Hao, "Lenses on curved surfaces," *Opt. Lett.*, vol. 39, no. 12, pp. 3551–3554, Jun 2014.

[25] R. F. Rinehart, "A solution of the problem of rapid scanning for radar antennae," *J. Appl. Phys.*, vol. 19, p. 860–862, Sept. 1948.

[26] M. Šarbort and T. Tyc, "Spherical media and geodesic lenses in geometrical optics," *J. Opt.*, vol. 14, no. 7, p. 075705, 2012.

[27] K. S. Kunz, "Propagation of microwaves between a parallel pair of doubly curved conducting surfaces," *J. Appl. Phys.*, vol. 25, no. 5, pp. 642–653, 1954.

[28] Q. Liao, N. J. G. Fonseca, and O. Quevedo-Teruel, "Compact multibeam fully-metallic geodesic Luneburg lens antenna based on non-Euclidean transformation optics," *IEEE Trans. Antennas Propag.*, vol. 66, no. 12, pp. 7383–7388, 2018.

[29] N. J. G. Fonseca, "The water drop lens: Revisiting the past to shape the future," *EurAAP Reviews Electromagn.*, vol. 1, pp. 1–4, Jan. 2022.

[30] F. V. Vidarsson, O. Zetterstrom, A. Algaba-Brazález, N. J. G. Fonseca, M. Johansson, L. Manholm, and O. Quevedo-Teruel, "Conformal parallel plate waveguide polarizer integrated in a geodesic lens antenna," *IEEE Trans. Antennas Propag.*, in press.

[31] O. Zetterstrom, M. Petek, P. Castillo-Tapia, A. Palomares-Caballero, N. J. G. Fonseca, and O. Quevedo-Teruel, "V-band fully-metallic geodesic Luneburg lens antenna," *IEEE Trans. Antennas Propag.*, minor revision.

[32] E. Rajo-Iglesias, M. Ebrahimpouri, and O. Quevedo-Teruel, "Wideband phase shifter in groove gap waveguide technology implemented with glide-symmetric holey EBG," *IEEE Microw. Wirel. Compon. Lett*, vol. 28, no. 6, pp. 476–478, 2018.

[33] P.-S. Kildal, E. Alfonso, A. Valero-Nogueira, and E. Rajo-Iglesias, "Local metamaterial-based waveguides in gaps between parallel metal plates," *IEEE Antennas Wirel. Propag. Lett.*, vol. 8, pp. 84–87, 2009.

[34] A. U. Zaman and P.-S. Kildal, *GAP Waveguides*. Singapore: Springer Singapore, 2016, pp. 3273–3347.
[35] J. Liu, A. Vosoogh, A. U. Zaman, and J. Yang, "Design and fabrication of a high-gain 60-GHz cavity-backed slot antenna array fed by inverted microstrip gap waveguide," *IEEE Trans. Antennas Propag.*, vol. 65, no. 4, pp. 2117–2122, 2017.
[36] M. Ebrahimpouri, E. Rajo-Iglesias, Z. Sipus, and O. Quevedo-Teruel, "Cost-effective gap waveguide technology based on glide-symmetric holey EBG structures," *IEEE Trans. Microw. Theory Tech.*, vol. 66, no. 2, pp. 927–934, 2018.
[37] O. Quevedo-Teruel, Q. Chen, F. Mesa, N. J. G. Fonseca, and G. Valerio, "On the benefits of glide symmetries for microwave devices," *IEEE J. Microwaves*, vol. 1, no. 1, pp. 457–469, 2021.
[38] M. Ebrahimpouri, A. Algaba Brazalez, L. Manholm, and O. Quevedo-Teruel, "Using glide-symmetric holes to reduce leakage between waveguide flanges," *IEEE Microw. Wireless Compon. Lett.*, vol. 28, no. 6, pp. 473–475, 2018.
[39] Q. Chen, F. Mesa, X. Yin, and O. Quevedo-Teruel, "Accurate characterization and design guidelines of glide-symmetric holey EBG," *IEEE Trans. Microw. Theory Tech.*, vol. 68, no. 12, pp. 4984–4994, 2020.

Astrid Algaba-Brazález received her Telecommunication Engineering degree from Miguel Hernández University of Elche, Alicante, Spain, in 2009, and the Licentiate of Engineering and Ph.D. degrees from Chalmers University of Technology, Gothenburg, Sweden, in 2013 and 2015, respectively. She joined Ericsson Research in Gothenburg, in November 2014. She currently works as a Senior Researcher within the Integration and Electromagnetics section of Ericsson Research, with special focus on 5G and 6G antenna hardware projects. She has been also leading all research activities related to metasurfaces and lens antennas within Ericsson Research since 2015. Her research interests include millimeter and sub-millimeter antenna array technologies; lens antennas; design of microwave passive components such as filters; metasurfaces; integration of active components and antennas at millimeter-wave frequencies and design of interconnects and transitions to achieve such integration.

Dr. Algaba-Brazález received the second Best Paper Award at the International Symposium on Antennas and Propagation (ISAP) held in 2017, and the Best Paper Award in Antennas at the European Conference on Antennas and Propagation (EuCAP) held in 2020.

Pilar Castillo-Tapia received her bachelor's and master's degrees in telecommunications engineer from the University of Zaragoza, Spain, in 2017 and 2019 respectively. She is currently pursuing her PhD degree in highly-efficient integrated millimeter band antennas at KTH Royal Institute of Technology, Sweden. Her current research interests include lens antennas, transformation optics and metasurfaces possessing higher symmetries.

Lars Manholm received his M.Sc. degree in electrical engineering in 1994 and Licentiate of Technology degree in electromagnetics in 1998, both from Chalmers University of Technology, Gothenburg, Sweden.

He joined Ericsson Microwave Systems in Gothenburg as an antenna designer in 1998 and Ericsson Research, Gothenburg in 2003 where he holds a position as a Master Researcher in antenna hardware. His research interests include electronically steerable antennas and antenna arrays for cellular base station and fixed radio link applications at microwave and millimeter wave frequencies.

Oskar Zetterstrom received his B. Sc., M. Sc. and Lic. degrees in electrical and electromagnetic engineering from KTH, Royal Institute of Technology, Stockholm, Sweden in 2016, 2019, and 2021, respectively. Since 2019, he works towards his Ph. D. degree on antennas and electromagnetics at the Division of Electromagnetic Engineering at KTH. Oskar's research has been focused on transformation optics, lens antennas, metamaterials possessing higher symmetries and leaky-wave antennas, and he has authored or co-authored over 60 peer-reviewed journal and conference papers. He has been awarded the 1st price in the student design competition at APS/URSI 2016, the best student paper award at URSI Spain 2020, and the best antenna technology paper award at EuCAP 2022 for his works.

Oskar is also a member of the newly formed EurAAP working group for Early Careers in Antennas and Propagation (ECAP).

Martin Johansson (M'93-SM'06) received the M.Sc. degree in engineering physics and the Ph.D. degree in electromagnetics from Chalmers University of Technology in 1986 and 1997, respectively.

He joined Ericsson Research, Ericsson AB, Gothenburg, Sweden, in 1997, where he currently serves as an expert in antenna technology. His current research interests include antenna technology for mobile communications, antenna system modeling, and deterministic channel modeling.

Nelson J. G. Fonseca (Senior Member, IEEE) received the M.Eng. degree from Ecole Nationale Supérieure d'Electrotechnique, Electronique, Informatique, Hydraulique et Télécommunications (ENSEEIHT), Toulouse, France, in 2003, the M.Sc. degree from the Ecole Polytechnique de Montreal, Quebec, Canada, also in 2003, and the PhD degree from Institut National Polytechnique de Toulouse – Université de Toulouse, France, in 2010, all in electrical engineering.

He currently works as an Antenna Engineer for the Antenna and Sub-Millimetre Waves Section, European Space Agency (ESA), Noordwijk, The Netherlands. Since November 2020, he also holds an Honorary Appointment as Professional Fellow at the University of Technology Sydney (UTS), Australia. His research interests include multiple beam antennas for space missions, beam-former theory and design, ground terminal antennas and novel manufacturing techniques. He has authored or co-authored more than 270 papers in peer-reviewed journals and conferences, and has over 50 patents issued or pending.

Dr. Fonseca is currently serving as the Chair of the IEEE MTT-S Technical Committee 29 (TC-29) on Microwave Aerospace Systems. He is a board member of the European School of Antennas and Propagation (ESoA) since January 2019 and is also serving as coordinator of the ESA/ESoA course on Antennas for Space Applications. He is the elected EurAAP Regional Delegate representing Benelux for the term 2021-2023. He received several prizes and awards, including the Best Young Engineer Paper Award at the 29th ESA Workshop on Antennas in 2007, an ESA Teamwork Excellence Award in 2020, multiple ESA Technical Improvement Awards and the Best Applied Technology Antenna Paper Award at EuCAP 2022.

O. Quevedo-Teruel (Senior Member, IEEE) received his Telecommunication Engineering and PhD Degrees from Carlos III University of Madrid, Spain in 2005 and 2010. From 2010-2011, Dr. Quevedo-Teruel joined the Department of Theoretical Physics of Condensed Matter at Universidad Autonoma de Madrid as a research fellow and went on to continue his postdoctoral research at Queen Mary University of London from 2011-2013.

In 2014, he joined the Division of Electromagnetic Engineering in the School of Electrical Engineering and Computer Science at KTH Royal Institute of Technology in Stockholm, Sweden where he is a Professor and Director of the Master Programme in Electromagnetics Fusion and Space Engineering. He has been an Associate Editor of the IEEE Transactions on Antennas and Propagation from 2018-2022 and Track Editor since 2022. He is also the founder and editor-in-chief of the EurAAP journal Reviews of Electromagnetics since 2020. He was the EurAAP delegate for Sweden, Norway, and Iceland from 2018-2020 and he has been a member of the EurAAP Board of Directors since January 2021. Since January 2022, he is the vice-chair of EurAAP.

He was a distinguished lecturer of the IEEE Antennas and Propagation Society for the period of 2019-2021. He is the Chair of the IEEE APS Educational Initiatives Programme since 2020.

He has made scientific contributions to higher symmetries, transformation optics, lens antennas, metasurfaces, leaky wave antennas and high impedance surfaces. He is the co-author of more than 110 papers in international journals and 180 at international conferences.